Charge Density Wave and Superconductivity in the Disordered Holstein Model

B. Xiao,[1,2] N.C. Costa,[3,4] E. Khatami,[5] G. G. Batrouni,[6,7,8,9] and R.T. Scalettar[1]

[1]*Department of Physics, University of California, Davis, California 95616, USA*
[2]*Center for Computational Quantum Physics, Flatiron Institute, New York, New York 10010, USA*
[3]*Instituto de Física, Universidade Federal do Rio de Janeiro Cx.P. 68.528, 21941-972 Rio de Janeiro RJ, Brazil*
[4]*International School for Advanced Studies (SISSA), Via Bonomea 265, 34136, Trieste, Italy*
[5]*Department of Physics and Astronomy, San José State University, San José, California 95192, USA*
[6]*Université Côte d'Azur, CNRS, INPHYNI, 0600 Nice, France*
[7]*Centre for Quantum Technologies, National University of Singapore, 2 Science Drive 3, 117542 Singapore*
[8]*Department of Physics, National University of Singapore, 2 Science Drive 3, 117542 Singapore*
[9]*Beijing Computational Science Research Center, Beijing 100193, China*

The interplay between electron-electron correlations and disorder has been a central theme of condensed matter physics over the last several decades, with particular interest in the possibility that interactions might cause delocalization of an Anderson insulator into a metallic state, and the disrupting effects of randomness on magnetic order and the Mott phase. Here we extend this physics to explore *electron-phonon* interactions and show, via exact quantum Monte Carlo simulations, that the suppression of the charge density wave correlations in the half-filled Holstein model by disorder can stabilize a superconducting phase. Our simulations thus capture qualitatively the suppression of charge ordered phases and emergent superconductivity recently seen experimentally.

Introduction. Although the problem of the localizing effect of randomness on *non-interacting* electrons is well understood [1–3], the combined effects of disorder and electron-electron interactions remain an area of continued theoretical and experimental interest [4–11]. A traditional focus has been on the possibility of electron-electron interactions inducing an insulator-to-metal transition in two dimensions [12], but recent attention has also turned to understanding the interplay in the context of modern developments including Majorana fermions [13], topological bands [14], ultracold atomic gases [15], and many-body localization [16–18]. Supplementing analytic calculations, numerical approaches have attempted to address the issue with techniques which treat disorder and electronic correlations non-perturbatively [19, 20]. Unfortunately, in quantum Monte Carlo (QMC) methodologies, the combination of randomness and interactions often leads to the fermion minus-sign problem, a bottleneck which dramatically limits their effectiveness [21–23].

In this work, we use an exact sign-problem-free QMC approach to investigate the interplay between randomness and *electron-phonon interactions*. This is an area far less explored with numerical simulations than that of randomness and electron-electron interactions. This gives us the opportunity, within the framework of the disordered Holstein model, to address important fundamental qualitative issues. Among them, we find the emergence of a superconducting (SC) phase upon the suppression of the charge-density wave (CDW) order by randomness. Further, the absence of the sign problem allows us to reach low temperatures, and thus use the full power of QMC calculations which cannot be fully exploited for electron-electron interactions.

This paper is organized as follows: After describing our Hamiltonian and methodology in the "Model" and "Methods" sections, respectively, we show in the "Results" section the details of the quantum simulations which lead to a demonstration of the emergence of a SC phase driven by the interplay of electron-phonon interaction and randomness. Our final remarks are in the "Concluding remarks" section. Further results about the magnitude of SC and CDW correlations in the full temperature-disorder plane are presented in the Supplemental Materials.

Model. The Holstein model describes itinerant electrons whose site density couples to the displacement of a local phonon mode. Its Hamiltonian reads

$$\mathcal{H} = -t \sum_{\langle \mathbf{i,j} \rangle, \sigma} \left(d_{\mathbf{i}\sigma}^\dagger d_{\mathbf{j}\sigma} + \text{h.c.} \right) - \sum_{\mathbf{i},\sigma} (\mu - \epsilon_{\mathbf{i}}) n_{\mathbf{i},\sigma}$$
$$+ \omega_0 \sum_{\mathbf{i}} a_{\mathbf{i}}^\dagger a_{\mathbf{i}} + g \sum_{\mathbf{i},\sigma} n_{\mathbf{i}\sigma} \left(a_{\mathbf{i}}^\dagger + a_{\mathbf{i}} \right) \quad , \tag{1}$$

in which the sum over $\mathbf{i}$ is on a two-dimensional square lattice, with $\langle \mathbf{i,j} \rangle$ denoting nearest-neighbors. $d_{\mathbf{i}\sigma}^\dagger$ ($d_{\mathbf{i}\sigma}$) is the creation (annihilation) operator of electrons with spin σ at site $\mathbf{i}$, with $n_{\mathbf{i}\sigma} \equiv d_{\mathbf{i}\sigma}^\dagger d_{\mathbf{i}\sigma}$ denoting the number operator. $a_{\mathbf{i}}^\dagger (a_{\mathbf{i}})$ is the phonon creation (annihilation) operator. The first term on the right hand side of Eq. (1) corresponds to the hopping of electrons, and the second term contains the global chemical potential μ. Disorder effects are introduced in the second term, by means of random on-site energies $\epsilon_{\mathbf{i}}$, chosen uniformly in the range $[-\Delta/2, \Delta/2]$, so that Δ/t represents the dimensionless disorder strength. Local phonon modes, with energy ω_0, are included in the third term. Finally, the last term describes their coupling to electrons, with strength g.

It is worth noticing that the square lattice dispersion relation has a number of special features, such as a perfect nesting and a van-Hove singularity in the density of states (at half-filling), which lead to CDW order at weak electron-phonon coupling. For stronger coupling cases, the occurrence of CDW order is less dependent on

the Fermi surface features, and its behavior on a square lattice is generic, e.g. with CDW transition temperatures being similar to those on other 2D bipartite lattices [24–27]. In this work, we analyze both weak and strong coupling regimes at half-filling, $\langle n_{\mathbf{i}\sigma} \rangle = 1/2$, which is obtained by fixing $\mu = -2g^2/\omega_0$, regardless of the lattice size or temperature, due to an appropriate particle-hole symmetry. We further set $t = 1$ to represent the unit of energy, and use units where $\hbar = k_B = 1$. We also define $\lambda_D = g^2/(zt\omega_0)$ as the dimensionless electron-phonon coupling, where $z = 4$ is the coordination number for the square lattice. In what follows, we consider two cases: [i] the adiabatic case, with $\omega_0/t = 1/2$ and an intermediate coupling strength $\lambda_D = 1/2$ ($g = 1$); and [ii] the anti-adiabatic case, with $\omega_0/t = 4$ and a weak coupling strength $\lambda_D = 1/4$ ($g = 2$).

Methods. We employ the determinant quantum Monte Carlo (DQMC) method [28–31], an unbiased auxiliary-field approach that provides finite-temperature properties of interacting fermions. Within this approach, both equal-time and unequal-time quantities can be calculated. See [32] for more details.

Charge modulations are probed by analyzing the density-density correlation functions $\langle n_{\mathbf{i}} n_{\mathbf{j}} \rangle$, and their Fourier transform, the charge structure factor

$$S(\mathbf{q}) = \frac{1}{N} \sum_{\mathbf{i},\mathbf{j}} e^{i\mathbf{q}\cdot(\mathbf{r_i}-\mathbf{r_j})} \langle n_{\mathbf{i}} n_{\mathbf{j}} \rangle, \tag{2}$$

where $N = L^2$ is the number of lattice sites in the system. Similarly, superconducting properties are examined by means of the s-wave pairing susceptibility,

$$\chi_s = \frac{1}{N} \int_0^\beta d\tau \, \langle \Delta(\tau)\Delta^\dagger(0) \rangle, \tag{3}$$

in which $\beta = 1/T$ is the inverse temperature and $\Delta(\tau) = \sum_{\mathbf{i}} d_{\mathbf{i}\downarrow}(\tau)d_{\mathbf{i}\uparrow}(\tau)$, with $d_{\mathbf{i}\sigma}(\tau) = e^{\tau\mathcal{H}}d_{\mathbf{i}\sigma}e^{-\tau\mathcal{H}}$. Although the equal-time pairing correlations at large spatial separation can also be used to probe superconductivity, the full susceptibility provides a more sensitive measure, especially in the case of a Kosterlitz-Thouless transition, as expected to occur in 2D lattices [30, 33, 34].

Finally, we investigate transport properties by calculating a proxy of the direct current (dc) conductivity [19, 35]

$$\sigma_{dc} \approx \frac{\beta^2}{\pi} \Lambda_{xx}(\mathbf{q} = \mathbf{0}, \tau = \beta/2), \tag{4}$$

where $\Lambda_{xx}(\mathbf{q},\tau) = \langle j_x(\mathbf{q},\tau)j_x(-\mathbf{q},0) \rangle$ is the current-current correlation function, and $j_x(\mathbf{q},\tau)$ is the Fourier transform of $j_x(\mathbf{r},\tau) = -i\,t\,(d^\dagger_{\mathbf{r}+\hat{\mathbf{x}},\sigma}d_{\mathbf{r},\sigma} - d^\dagger_{\mathbf{r},\sigma}d_{\mathbf{r}+\hat{\mathbf{x}},\sigma})(\tau)$. We carry out the calculations on lattices sizes from 6×6 to 12×12, and average our expectation values over 110 disorder realizations.

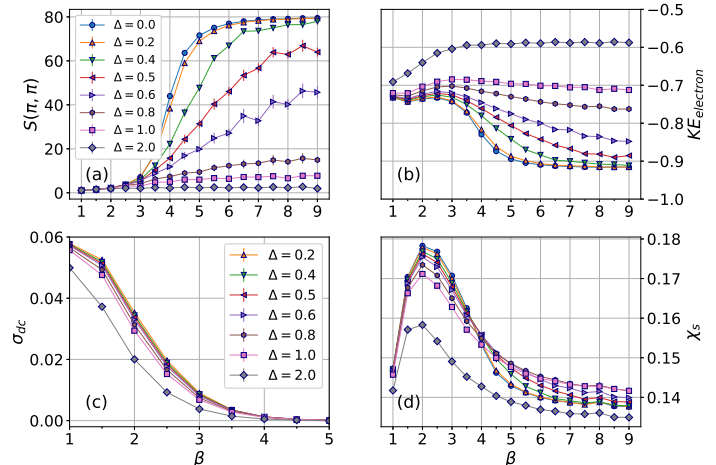*Results.* We first consider the response of charge modulations to disorder in the adiabatic case, by fixing

Figure 1. The (a) charge structure factor, (b) kinetic energy of electrons (c) dc conductivity and (d) s-wave pair susceptibility as functions of the inverse temperature, and for different disorder strength, at fixed $L = 10$, $\omega_0 = 0.5$, and $\lambda_D = 0.5$ ($g = 1$). Results are shown for the dc conductivity only for larger Δ, where Eq. 4 is valid[35].

$\omega_0/t = 0.5$ and $\lambda_D = 1/2$ ($g = 1$). When $\Delta = 0$, there is a large enhancement of $S(\pi,\pi)$ around $\beta \approx 4$, as presented in Fig. 1 (a), in line with recent studies [36, 37] that show a CDW transition at $\beta_c = 4.1 \pm 0.1$ (see also SM). In presence of weak disorder, $\Delta \lesssim 0.3t$, the behavior of $S(\pi,\pi)$ is only slightly changed from that of the clean system, suggesting the continued existence of long-range charge correlations over length scales up to the lattice sizes being simulated, as displayed in Fig. 1 (a). However, as disorder increases further, $S(\pi,\pi)$ has its characteristic energy scale shifted to larger β (lower temperature), and its strength reduced. Eventually, for $\Delta \approx t$, long-range correlations seem entirely destroyed, even at very low temperatures.

At this point, it is convenient to estimate the size of Δ needed to break charge order. From a second order perturbation theory [38], the effective attraction between electrons is given by $U_{\text{eff}} = -2g^2/\omega_0$, therefore the CDW scale may be estimated as $4t^2/|U_{\text{eff}}| = 2t^2\omega_0/g^2$. Given this, when Δ exceeds some fraction of this value, one should expect the charge correlations to be suppressed. Indeed, this yields $\Delta_c \lesssim 1$ for $\omega_0 = 0.5$, $g = 1$, in rough agreement with the vanishing of the CDW correlations for $\Delta \gtrsim 0.5$, displayed in Fig. 1 (a).

Further insight into this crossover is provided by the behavior of the electronic kinetic energy, exhibited in Fig. 1 (b). At weak disorder, despite the occurrence of a Peierls-like charge gap, the alternation of empty and doubly occupied sites associated with strong CDW correlations promotes charge fluctuations, and hence the magnitude of the kinetic energy increases as the temperature is lowered. By contrast, in the strong
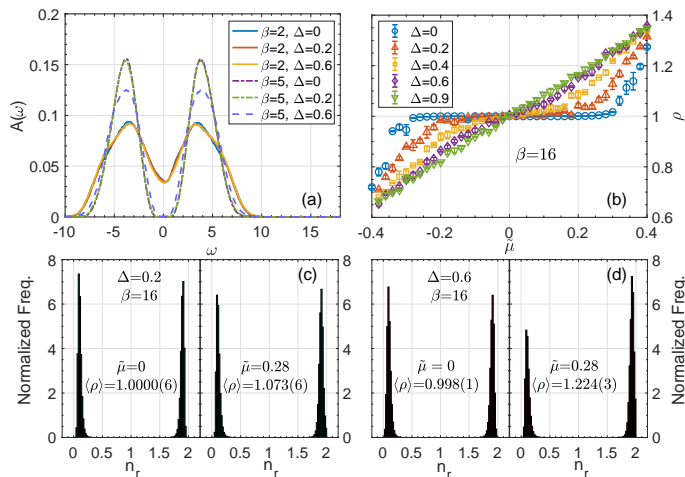
Figure 2. The (a) density of states as a function of energy, (b) electron density, ρ, as a function of shifted chemical potential, $\tilde{\mu} = \mu + 2g^2/\omega_0$, and the electron distribution at half-filling (Left) and (Right) away from half-filling at fixed (c) $\Delta = 0.2$ and (d) $\Delta = 0.6$. $L = 10$, $\omega = 0.5$ and $\lambda_D = 0.5$ ($g = 1$).

Figure 3. The (a) charge structure factor $S(\pi, \pi)$, (b) s-wave pairing susceptibility χ_s as a function of disorder strength Δ, at fixed $\beta = 30$, $\omega_0 = 4$, and $\lambda_D = 1/4$ ($g = 2$). Inset: The normalized pairing susceptibility χ_s/L^2 as a function of $1/L$ at $\Delta = 0.7$.

disordered case, the pairs are localized randomly, with some doublons at adjacent sites, precluding virtual hopping. As a consequence, the kinetic energy decreases in magnitude as $T \to 0$. Despite the suppression of the CDW order, Fig. 1 (c) shows that the conductivity decreases as T is lowered, with $d\sigma_{\rm dc}/dT > 0$, indicating an insulating behavior for all values of Δ. In line with this, the pairing susceptibility, shown in Fig. 1 (d), remains small for all Δ, suggesting that local electron pairs are not correlated.

We now characterize in more detail the large Δ behavior. Figure 2 (a) shows the spectral function $A(\omega)$, obtained via the analytic continuation of $G(\mathbf{q}, \tau) = \langle \mathcal{T} d(\mathbf{q}, \tau) d^\dagger(\mathbf{q}, 0) \rangle = \int_{-\infty}^{\infty} d\omega \frac{e^{-\tau \omega}}{1 + e^{-\beta \omega}} A(\mathbf{q}, \omega)$, where $\mathcal{T}$ is the imaginary time ordering operator, and $A(\omega)$ sums over all momenta; see, e.g., the SM. The spectral weight at the Fermi level is suppressed at low T, with an opening of a single-particle gap. This occurs for both clean and disordered cases, even for large disorder, where the CDW has been completely destroyed, suggesting an insulating behavior for any disorder strength. Typically, the opening of such gaps in $A(\omega)$ is associated with a vanishing compressibility $\kappa = d\rho/d\mu$. This happens, e.g., in the half-filled fermionic Hubbard model, both in the weak-coupling Slater and strong-coupling Mott regimes. Similarly, in our disordered Holstein model the compressibility also vanishes at weak disorder, as shown in Fig. 2 (b). However, at large Δ, the gap in $A(\omega)$ is *not* accompanied by $\kappa = 0$. As displayed in Fig. 2 (b), the plateau in $\rho(\mu)$ is substantially smeared at $\Delta/t \sim 0.4$, and completely destroyed at $\Delta/t \sim 0.6$.

In both band and Mott insulators, $A(\omega) = 0$ and $\kappa = 0$ go hand-in-hand. The unusual behavior whereby $A(\omega = 0) = 0$ but $\kappa \neq 0$ derives from the fact that the effective
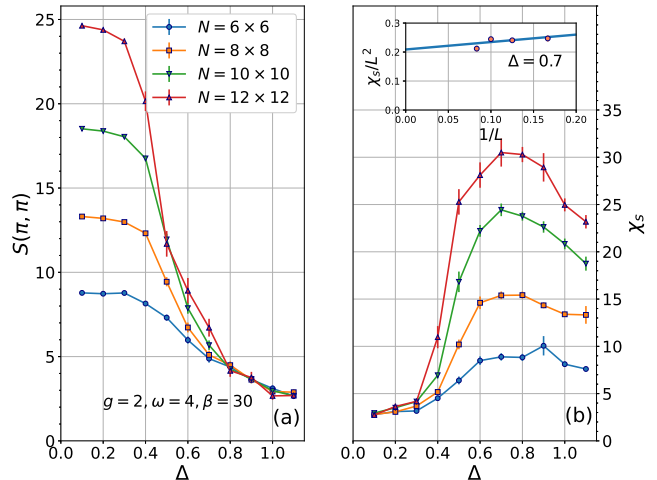
local attractive interaction, due to phonon modes, favors the addition of pairs of fermions to the system, while resisting the addition of individual ones. This picture is supported by analyzing the electron distribution on the lattice during the Monte Carlo simulations. In Figs. 2 (c)-(d), histograms of the local density $n_{\mathbf{r}}$ are sharply peaked around 0 and 2 but not 1 for all disorder strengths, indicating that we mostly have doubly occupied or empty sites. Similar distributions are also observed away from half-filling. For instance, fixing $\tilde{\mu} = \mu + 2g^2/\omega_0 = 0.28$, and comparing the electron distribution at $\Delta/t = 0.2$ with $\Delta/t = 0.6$, the same chemical potential adds more pairs of electrons into the system and causes a more distinguished imbalance between empty and doubly occupied sites at larger disorder. This supports the picture that adding pairs of electrons is the mechanism by which the system responds to increasing μ. Unlike the repulsive Hubbard model, where the electron-electron interaction U favors moment formation (singly occupied sites) and the random site energies favor pairs, here the electron-phonon interaction, g, and Δ both promote binding. Together, the properties shown in Fig. 2 point to an insulating phase characterized by a gapless fermion pair excitation, but a gapped spectrum for single particle ones.

We now discuss the anti-adiabatic regime, fixing $\omega_0/t = 4$ and $\lambda_D = 1/4$ ($g = 2$). Figure 3 (a) shows the evolution of $S(\pi, \pi)$ with disorder, at a fixed low temperature $T/t = 1/30$. As in the adiabatic regime, increasing Δ strongly suppresses the charge response, destroying the CDW phase. However, in stark contrast with the former case, here the behavior of the pair

susceptibility is dramatically different: χ_s is two orders of magnitude larger, and exhibits a peak around $\Delta/t = 0.7$, as displayed in Fig. 3 (b). The magnitude of these charge structure factors and superconducting susceptibilities are consistent with those of their magnetic and pairing analogs indicating long range order in the repulsive [39] and attractive Hubbard models [34, 40, 41]. Although these large values of χ_s are suggestive, finite size scaling (FSS) is required to establish the nature of the phase. One approach to this FSS is to take data at very low temperatures, such as $T/t = 1/30$ in Fig. 3 so that one is essentially at $T = 0$, on the simulated lattice size for that value of randomness. The inset of Fig. 3 (b) shows that χ_s/L^2, at $\Delta/t = 0.7$, has a finite value when extrapolated to $L \to \infty$, corresponding to long-range order and a divergence of χ_{pairing} in the thermodynamic limit. The qualitative picture is that, for these parameters, disorder drives a SC state at commensurate filling as charge correlations are suppressed, and new energy states are created near the Fermi surface for pairing. Given this, the results of these QMC simulations is a crossover from a phase consisting of CDW-puddles to a SC ordered one.

A more refined FSS analysis proceeds as follows: We expect the 2D superconducting transition suggested by the data of Fig. 3 to be in the Kosterlitz-Thouless universality class. Thus the pair susceptibility $\chi_s \sim L^{2-\eta(T)}$ with a temperature-dependent exponent $\eta(T)$. At the KT transition point $\eta(T_c) = 1/4$ and $\eta(T) \to 0$ in the ground state. Meanwhile, for $T > T_{KT}$, the pair correlations decay exponentially on sufficiently large lattices, therefore $\chi_s \sim L^0$ according to Eq. (3), i.e. $\eta = 2$. Figure 4 shows the results for such FSS analysis, in which we have used plots of $\ln(\chi_s)$ versus $\ln(L)$ to extract η_{eff} at the fixed temperatures $T/t = 1/20, 1/30$ of the simulations, as displayed in the inset. We refer to this as an 'effective' η to acknowledge finite size effects. The main panel of Figure 4 shows η_{eff} at these two temperatures as a function of disorder Δ. At small Δ, deep in the CDW phase, pairing correlations decay rapidly and we see the expected $\eta_{\text{eff}} = 2$. For $T/t = 1/20$, η_{eff} comes down rapidly as disorder strength is increased, indicative of pairing correlations that are approaching the size of the lattice. However, η_{eff} still exceeds the universal KT value $\eta_{\text{eff}}(T_c) = 1/4$ for all Δ. There is no superconductivity at this temperature. For $T/t = 1/30$, on the other hand, $\eta_{\text{eff}} < 1/4$ in a range of intermediate Δ. In this window, $T = 1/30 < T_c$ and the system is in a superconducting phase. The error bars are conservatively estimated, and represent a complex combination of statistical uncertainty for individual disorder realizations, the disorder averaging, and uncertainty associated with the FSS fit to extract η.

The overall picture which emerges from Figs. 3 and 4 is that substantial charge correlations are present at $T/t \lesssim 1/10$ in the weak disorder region, $\Delta/t \lesssim 0.5$, while a SC dome emerges for stronger disorder values at $T/t \lesssim 1/20$. The issue of how the CDW and SC phases meet at temperatures below $T = 0.033$ is beyond the
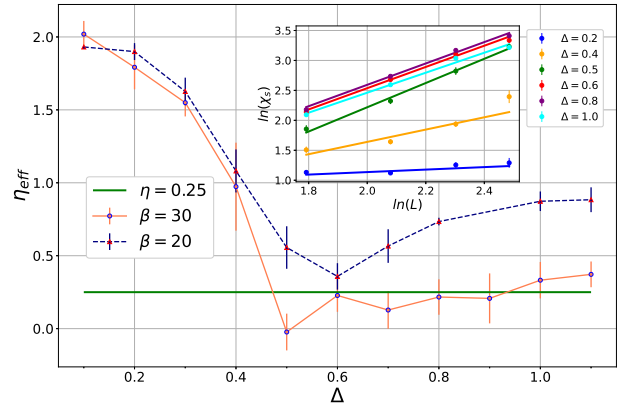

Figure 4. The effective KT power law $\eta_{\text{eff}}(T)$ is shown as a function of disorder Δ for two fixed low temperatures. $\eta_{\text{eff}}(T) < 1/4$ for $T/t = 1/30$ in a range of intermediate Δ, suggesting a superconducting state.

scope of the present set of simulations. The heat maps of Fig. S1 of the SM suggest that there is a narrow region where both $S(\pi,\pi)$ and χ_s are large. However, while we are able to perform definitive FSS analysis within the individual CDW and SC phases, the corresponding data at the interface between them do not provide an unambiguous conclusion. Furthermore, the coupling of random fields to the CDW order parameter prevents the occurrence of true diagonal long-range order [11]. Notwithstanding, the emergence of SC is allowed in the ground state, as indicated by our FSS analysis, and also emphasized in the heat map presented in the SM.

Concluding Remarks. Although the two parameter regimes for which we have presented results are distinguished by the value of ω_0/t, we believe the qualitative explanation for the difference in behavior, i.e. the presence of an intermediate SC phase, lies in the fact that the former corresponds to an intermediate and the latter to a weak dimensionless coupling. For strong and intermediate couplings, the composite electron-phonon polarons are small, and hence easily localized by disorder. At weak dimensionless coupling, the polarons are much larger, and the disorder potential is therefore to some extent averaged out over their volume. Thus, after Δ destroys the CDW, it does not yet localize the pairs, which remain mobile and condense into a SC phase.

Tuning between CDW and paired phases can be accomplished via pressure or doping, and is a phenomenon which also has been extensively explored experimentally. Analogies between antiferromagnetic-SC and CDW-SC phases have also been remarked [29, 42]. However, the latter transition has received much less attention from the QMC community. Early work on the doping-driven CDW-SC transition in the Holstein model [43, 44] has been extended to transitions at commensurate filling caused by the introduction of

band dispersion [45], and a comparison with Migdal-Eliashberg theory [46]. Additional QMC literature has also considered the interplay between electron-electron and electron-phonon interactions, as in the Hubbard-Holstein model [47–52].

This paper has described a detailed QMC study of the effect of disorder on the CDW transition, and shown that, in certain parameter regimes, randomness can give rise to a SC state. Earlier work has suggested that the electron-phonon coupling can renormalize the disorder potentials, leading to a ground state that may not exhibit Anderson localization [53–56]. The present study suggests an even more subtle consequence of the disorder-interaction interplay, the emergence of a off-diagonal ordered phases from diagonal disorder at commensurate filling.

We expect our results to apply quite generally to the Holstein model on other bipartite geometries (e.g. 3D cubic) where CDW order is dominant at half-filling [25, 26, 52]. The honeycomb lattice might be particularly interesting to investigate, since it has a quantum critical point for couplings below which CDW order is absent.

SC might still emerge with added disorder in this semi-metallic regime from the filling up of the density of states, which vanishes linearly in the clean limit. We also expect our results to apply generally to different choices of λ, ω_0 which have the same λ_D [57]. In the clean case, the CDW transition temperature has recently been found as as a function of λ_D [24–26], a feature whose behavior with randomness would be interesting to examine in future work.

[1] Elihu Abrahams, PW Anderson, DC Licciardello, and TV Ramakrishnan, "Scaling theory of localization: Absence of quantum diffusion in two dimensions," Phys. Rev. Lett. **42**, 673 (1979).

[2] Franz Wegner, "Inverse participation ratio in 2+ ε dimensions," Zeitschrift für Physik B Condensed Matter **36**, 209–214 (1980).

[3] K.B. Efetov, A.I. Larkin, and D. E. Khmelnitskii, Sov. Phys. JETP **52**, 568 (1980).

[4] Patrick A. Lee and T. V. Ramakrishnan, "Disordered electronic systems," Rev. Mod. Phys. **57**, 287–337 (1985).

[5] T. Giamarchi and H. J. Schulz, "Anderson localization and interactions in one-dimensional metals," Phys. Rev. B **37**, 325–340 (1988).

[6] D. Belitz and T. R. Kirkpatrick, "The Anderson-Mott transition," Rev. Mod. Phys. **66**, 261–380 (1994).

[7] Elbio Dagotto, "Complexity in strongly correlated electronic systems," Science **309**, 257–262 (2005).

[8] A. V. Balatsky, I. Vekhter, and Jian-Xin Zhu, "Impurity-induced states in conventional and unconventional superconductors," Rev. Mod. Phys. **78**, 373–433 (2006).

[9] E. Abrahams, 50 Years of Anderson Localization (World Scientific, 2010).

[10] V. Dobrosavljevic, N. Trivedi, and James M Valles Jr, Conductor-insulator quantum phase transitions (Oxford University Press, Oxford, UK, 2012).

[11] T. Vojta, "Disorder in quantum many-body systems," Annual Review of Condensed Matter Physics **10**, 233–252 (2019).

[12] S.V. Kravchenko and M.P. Sarachik, "Metal–insulator transition in two-dimensional electron systems," Reports on Progress in Physics **67**, 1–44 (2003).

[13] Alejandro M. Lobos, Roman M. Lutchyn, and S. Das Sarma, "Interplay of disorder and interaction in majorana quantum wires," Phys. Rev. Lett. **109**, 146403 (2012).

[14] Akshay Krishna, Matteo Ippoliti, and R. N. Bhatt, "Localization and interactions in topological and nontopological bands in two dimensions," Phys. Rev. B **100**, 054202 (2019).

[15] S. S. Kondov, W. R. McGehee, J. J. Zirbel, and B. DeMarco, "Three-dimensional anderson localization of ultracold matter," Science **334**, 66–68 (2011).

[16] D. M. Basko, I. L. Aleiner, and B. L. Altshuler, Ann. Phys. (NY) **321**, 1126 (2006).

[17] R. Nandkishore and D. A. Huse, Annu. Rev. Condens. Matter Phys. **6**, 15 (2015).

[18] Yevgeny Bar Lev, Guy Cohen, and David R Reichman, "Absence of diffusion in an interacting system of spinless fermions on a one-dimensional disordered lattice," Phys. Rev. Lett. **114**, 100601 (2015).

[19] P. J. H. Denteneer, R. T. Scalettar, and N. Trivedi, "Conducting phase in the two-dimensional disordered Hubbard model," Phys. Rev. Lett. **83**, 4610–4613 (1999).

[20] H. Terletska, Y. Zhang, K-M. Tam, T. Berlijn, L. Chioncel, N.S. Vidhyadhiraja, and M. Jarrell, "Systematic quantum cluster typical medium method for the study of localization in strongly disordered electronic systems," Appl. Sci. **8**, 2401 (2018).

[21] E. Y. Loh, J. E. Gubernatis, R. T. Scalettar, S. R. White, D. J. Scalapino, and R. L. Sugar, "Sign problem in the numerical simulation of many-electron systems," Phys. Rev. B **41**, 9301–9307 (1990).

[22] M. Troyer and U-J. Wiese, "Computational complexity and fundamental limitations to fermionic quantum monte carlo simulations," Phys. Rev. Lett. **94**, 170201 (2005).

[23] V. I. Iglovikov, E. Khatami, and R. T. Scalettar, "Geometry dependence of the sign problem in quantum Monte Carlo simulations," Phys. Rev. B **92**, 045110 (2015).

[24] Manuel Weber and Martin Hohenadler, "Two-dimensional Holstein-Hubbard model: Critical temperature, Ising universality, and bipolaron liquid,"

Phys. Rev. B **98**, 085405 (2018).

[25] Y.-X. Zhang, W.-T. Chiu, N. C. Costa, G. G. Batrouni, and R. T. Scalettar, "Charge order in the Holstein model on a honeycomb lattice," Phys. Rev. Lett. **122**, 077602 (2019).

[26] Chuang Chen, Xiao Yan Xu, Zi Yang Meng, and Martin Hohenadler, "Charge-density-wave transitions of Dirac fermions coupled to phonons," Phys. Rev. Lett. **122**, 077601 (2019).

[27] B. Cohen-Stead, Kipton Barros, ZY Meng, Chuang Chen, R. T. Scalettar, and G. G. Batrouni, "Langevin simulations of the half-filled cubic Holstein model," Phys. Rev. B **102**, 161108 (2020).

[28] R. Blankenbecler, D. J. Scalapino, and R. L. Sugar, "Monte Carlo calculations of coupled boson-fermion systems. I," Phys. Rev. D **24**, 2278–2286 (1981).

[29] R. T. Scalettar, N. E. Bickers, and D. J. Scalapino, "Competition of pairing and Peierls–charge-density-wave correlations in a two-dimensional electron-phonon model," Phys. Rev. B **40**, 197–200 (1989).

[30] R. M. Noack, D. J. Scalapino, and R. T. Scalettar, "Charge-density-wave and pairing susceptibilities in a two-dimensional electron-phonon model," Phys. Rev. Lett. **66**, 778–781 (1991).

[31] R.R. dos Santos, "Introduction to quantum Monte Carlo simulations for fermionic systems," Brazilian Journal of Physics **33**, 36 – 54 (2003).

[32] See Supplemental Material for more details about the CDW-SC competition in the anti-adiabatic limit, the Determinant Quantum Monte Carlo method, CDW transition in the clean limit, specific heat, temperature dependence in the anti-adiabatic limit, and disorder dependence in the adiabatic limit.

[33] C. Huscroft and R. T. Scalettar, "Effect of disorder on charge-density wave and superconducting order in the half-filled attractive Hubbard model," Phys. Rev. B **55**, 1185–1193 (1997).

[34] T. Paiva, R.R. dos Santos, R.T. Scalettar, and P. J. H. Denteneer, "Critical temperature for the two-dimensional attractive Hubbard model," Phys. Rev. B **69**, 184501 (2004).

[35] Nandini Trivedi, Richard T. Scalettar, and Mohit Randeria, "Superconductor-insulator transition in a disordered electronic system," Phys. Rev. B **54**, R3756–R3759 (1996).

[36] C. Chen, X.Y. Xu, J. Liu, G. Batrouni, R. Scalettar, and Z.Y. Meng, "Symmetry-enforced self-learning Monte Carlo method applied to the Holstein model," Phys. Rev. B **98**, 041102 (2018).

[37] S. Li, P.M. Dee, E. Khatami, and S. Johnston, "Accelerating lattice quantum Monte Carlo simulations using artificial neural networks: Application to the Holstein model," Phys. Rev. B **100**, 020302 (2019).

[38] E. Berger, P. Valášek, and W. von der Linden, "Two-dimensional Hubbard-Holstein model," Phys. Rev. B **52**, 4806–4814 (1995).

[39] C.N. Varney, C.R. Lee, Z.J. Bai, S. Chiesa, M. Jarrell, and R.T. Scalettar, "Quantum Monte Carlo Study of the 2D Fermion Hubbard Model at Half-Filling," Phys. Rev. B **80**, 075116 (2009).

[40] R.T. Scalettar, E.Y. Loh, J.E. Gubernatis, A. Moreo, S.R. White, D.J. Scalapino, R.L. Sugar, and E. Dagotto, "Phase Diagram of the Two-Dimensional Negative U Hubbard Model," Phys. Rev. Lett. **62**, 1407 (1989).

[41] K. Bouadim, Y. L. Loh, M. Randeria, and N. Trivedi, "Single- and two-particle energy gaps across the disorder-driven superconductor-insulator transition," Nature Physics **7**, 884 (2011).

[42] I. Esterlis, S. Kivelson, and D. Scalapino, "A bound on the superconducting transition temperature," Nature Physics Journal, Quantum Materials **3**, 59 (2018).

[43] M. Vekić, R. M. Noack, and S. R. White, "Charge-density waves versus superconductivity in the Holstein model with next-nearest-neighbor hopping," Phys. Rev. B **46**, 271–278 (1992).

[44] J. K. Freericks, M. Jarrell, and D. J. Scalapino, "Holstein model in infinite dimensions," Phys. Rev. B **48**, 6302–6314 (1993).

[45] N. C. Costa, T. Blommel, W.-T. Chiu, G. Batrouni, and R. T. Scalettar, "Phonon dispersion and the competition between pairing and charge order," Phys. Rev. Lett. **120**, 187003 (2018).

[46] I. Esterlis, B. Nosarzewski, E. W. Huang, B. Moritz, T. P. Devereaux, D. J. Scalapino, and S. A. Kivelson, "Breakdown of the Migdal-Eliashberg theory: A determinant quantum Monte Carlo study," Phys. Rev. B **97**, 140501 (2018).

[47] S. Yamazaki, S. Hoshino, and Y. Kuramoto, "Continuous-Time Quantum Monte Carlo Study of Strong Coupling Superconductivity in Holstein-Hubbard Model," JPS Conf. Proc. **3**, 016021 (2014).

[48] S. Karakuzu, L.F. Tocchio, S. Sorella, and F. Becca, "Superconductivity, charge-density waves, antiferromagnetism, and phase separation in the Hubbard-Holstein model," Phys. Rev. B **96**, 205145 (2017).

[49] T. Ohgoe and M. Imada, "Competition among superconducting, antiferromagnetic, and charge orders with intervention by phase separation in the 2D Holstein-Hubbard model," Phys. Rev. Lett. **119**, 197001 (2017).

[50] Natanael C Costa, Kazuhiro Seki, Seiji Yunoki, and Sandro Sorella, "Phase diagram of the two-dimensional Hubbard-Holstein model," Communications Physics **3**, 1–6 (2020).

[51] Yao Wang, Ilya Esterlis, Tao Shi, J. Ignacio Cirac, and Eugene Demler, "Zero-temperature phases of the two-dimensional hubbard-holstein model: A non-gaussian exact diagonalization study," Phys. Rev. Research **2**, 043258 (2020).

[52] Natanael C. Costa, Kazuhiro Seki, and Sandro Sorella, "Magnetism and charge order in the honeycomb lattice," arXiv:2009.05586 (2020).

[53] F.X. Bronold and H. Fehske, "Anderson localization of polaron states," Phys. Rev. B **66**, 073102 (2002).

[54] H. Ebrahimnejad and M. Berciu, "Perturbational study of the lifetime of a Holstein polaron in the presence of weak disorder," Phys. Rev. B **86**, 205109 (2012).

[55] H. Ebrahimnejad and M. Berciu, "Trapping of three-dimensional Holstein polarons by various impurities," Phys. Rev. B **85**, 165117 (2012).

[56] O.R. Tozer and W. Barford, "Localization of large polarons in the disordered Holstein model," Phys. Rev. B **89**, 155434 (2014).

[57] Y. Zhang, C. Feng, G. Batrouni, and R. Scalettar, work in progress.

[58] M. Hohenadler and G. G. Batrouni, "Dominant charge-density-wave correlations in the Holstein model on the half-filled square lattice," Phys. Rev. **B100**, 165114

(2019).

[59] A. McMahan, C. Huscroft, R.T. Scalettar, and E.L. Pollock, "Volume Collapse transitions in the rare earth metals," J. of Computer-Aided Materials Design **5**, 131 (1998).

[60] T. Paiva, R. T. Scalettar, C. Huscroft, and A. K. McMahan, "Signatures of spin and charge energy scales in the local moment and specific heat of the half-filled two-dimensional Hubbard model," Phys. Rev. B **63**, 125116 (2001).

[61] M. Ulmke and R. Scalettar, "Magnetic Correlations in the Two Dimensional Anderson–Hubbard Model," Phys. Rev. B **55**, 4149 (1997).

[62] M. Ulmke, V. Janiš, and D. Vollhardt, "Anderson-Hubbard model in infinite dimensions," Phys. Rev. B **51**, 10411–10426 (1995).

[63] N.E. Bickers, D.J. Scalapino, and R.T. Scalettar, "Cdw and sdw mediated pairing mechanisms," Int. J. Mod. Phys. B **1**, 687 (1987).

[64] R. N. Silver, D. S. Sivia, and J. E. Gubernatis, "Maximum-entropy method for analytic continuation of quantum monte carlo data," Phys. Rev. B **41**, 2380–2389 (1990).

[65] J. E. Gubernatis, Mark Jarrell, R. N. Silver, and D. S. Sivia, "Quantum monte carlo simulations and maximum entropy: Dynamics from imaginary-time data," Phys. Rev. B **44**, 6011–6029 (1991).

[66] Anders W. Sandvik, "Stochastic method for analytic continuation of quantum monte carlo data," Phys. Rev. B **57**, 10287–10290 (1998).

These Supplemental Materials provide additional details concerning the CDW-SC competition in the anti-adiabatic limit, the Determinant Quantum Monte Carlo method, CDW transition in the clean limit, specific heat, temperature dependence in the anti-adiabatic limit, and disorder dependence in the adiabatic limit.

A: CDW and SC competition in the anti-adiabatic regime- In Fig. S1 we plot the heat maps of charge structure factor $S(\pi, \pi)$ and χ_s for the anti-adiabatic case ($\omega_0 = 4$), with weak effective electron-phonon coupling ($\lambda_D = 0.25$). These show the nature of the dominant correlations in the disorder strength-temperature plane. Therefore, the combination of $S(\pi, \pi)$ and χ_s serves as the phase diagram at finite temperature. The issue of how the CDW and SC phase meet at temperature below $T = 0.03$ is beyond the scope of the present set of simulations. At low enough temperature, charge order dominates. Increasing the strength of disorder suppresses the CDW. Instead, SC emerges as the disorder strength increases at $T < t/20$. Further increase of disorder strength ultimately suppresses the SC phase. These data suggest there might be a narrow region where CDW and SC exist simultaneously. However, conclusive evidence for this would require a simultaneous finite size extrapolation of $S(\pi, \pi)$ and χ_s which is beyond the capability of the simulations at present.

B: Determinant Quantum Monte Carlo- The Holstein Hamiltonian is quadratic in the fermion degrees of freedom. Hence they can be traced out analytically, leaving an expression for the partition function which depends on the space-imaginary time configuration $x_i(\tau)$ of the quantum oscillator degrees of freedom [28–31]. The explicit results of the trace operation are determinants, one for each of the two spin species. Because the coupling is symmetric in the spin index, these two determinants are identical. Their product is a square, and there is no sign problem in the simulations, for any value of the parameters in the Hamiltonian, filling, temperature, or lattice size. All equal imaginary time observables can be expressed in terms of elements (or products thereof) of the inverse of the matrix whose determinant is being sampled. Hence such measurements are very inexpensive computationally. Unequal time measurements, including those of the pair susceptibility and conductivity, require a separate computation of the un-equal time Greens function, and add considerably to the simulation time.

C: CDW transition in the clean limit- In the absence of randomness, $\Delta = 0$, the half-filled square lattice Holstein model is believed to undergo a CDW transition for all values of λ and ω_0 as a consequence of the nesting[58] of the Fermi surface and the divergence of the density of states. Fig. S2(a) gives raw data for the CDW structure factor as a function of inverse temperature β for four lattice sizes at $g = 1$ and $\omega_0 = 0.5$. At high temperatures (small β) the density-density

correlation function is short ranged, only a few local terms contribute to the sum in Eq. 2 and $S(\pi, \pi)$ is independent of lattice size. At low temperatures (large β) the density correlations extend over the entire lattice and $S(\pi, \pi)$ grows linearly with volume $N = L \times L$. Fig. S2(b) presents the same data scaled with the 2D Ising critical exponents, yielding a value for the transition temperature $T_c \sim 0.24 = 1/\beta_c$.

D: Relation to Attractive Hubbard Model- In light of the known mapping between the Holstein and Hubbard models in the anti-adiabatic (large ω_0) limit, it is important to emphasize how our work is distinct from the previous body of work on the disordered attractive Hubbard model [41]. Figure S4 addresses this issue. It compares the Hubbard and Holstein values for the nearest neighbor density-density and pair-pair correlations on a dimer. The clean case is shown in panel (a) and with a site energy difference in panel (b). We have chosen an interaction strength $U = -2$ for the attractive Hubbard Hamiltonian, and vary g and ω_0 together in such a way as to keep $U_{\text{eff}} = -2g^2/\omega_0 = -2$ fixed for the Holstein model. While it is true that for $\omega_0/t \to \infty$ the two models yield the same correlation functions, it is seen that this limit is only attained for $\omega_0/t \gtrsim 10^2$. Even though the frequencies reported here, $1 < \omega_0/t < 4$ are already high compared to typical phonon frequencies in real materials, it is clear we are still very far from the Hubbard limit. Not only are the correlation function values different (by an order of magnitude in the case of the pairing), but the CDW-pairing degeneracy of the Hubbard model limit is dramatically broken. These results demonstrate that the interplay of disorder and interactions presented here for the Holstein model are expected to be quite different from the attractive Hubbard model.

Another perspective on the similarities and differences is offered by considering the interaction between electron mediated by the exchange of a phonon propagator,

$$D(\omega) = \frac{2g^2\omega_0}{\omega^2 - \omega_0^2} \ . \tag{5}$$

From this expression it is clear that in the limit $\omega_0 >> \omega$ one recovers an instantaneous attractive interaction whose value matches that of U_{eff}. Conversely, as one moves away from this anti-adiabatic limit the electron-phonon interaction will contain frequency dependence not present in the attractive Hubbard coupling.

In discussing the relation between the two Hamiltonians, it is worth noting that at low density the Holstein model describes phenomena such as polaron formation, where a single electron moving on the lattice has a larger effective mass due to the phonon distortions it carries. This sort of physics is not captured by the attractive Hubbard model. Even though polaron formation tends to be studied in the dilute limit, the larger effective mass due to electron phonon coupling is likely to affect the physics of CDW and SC order at
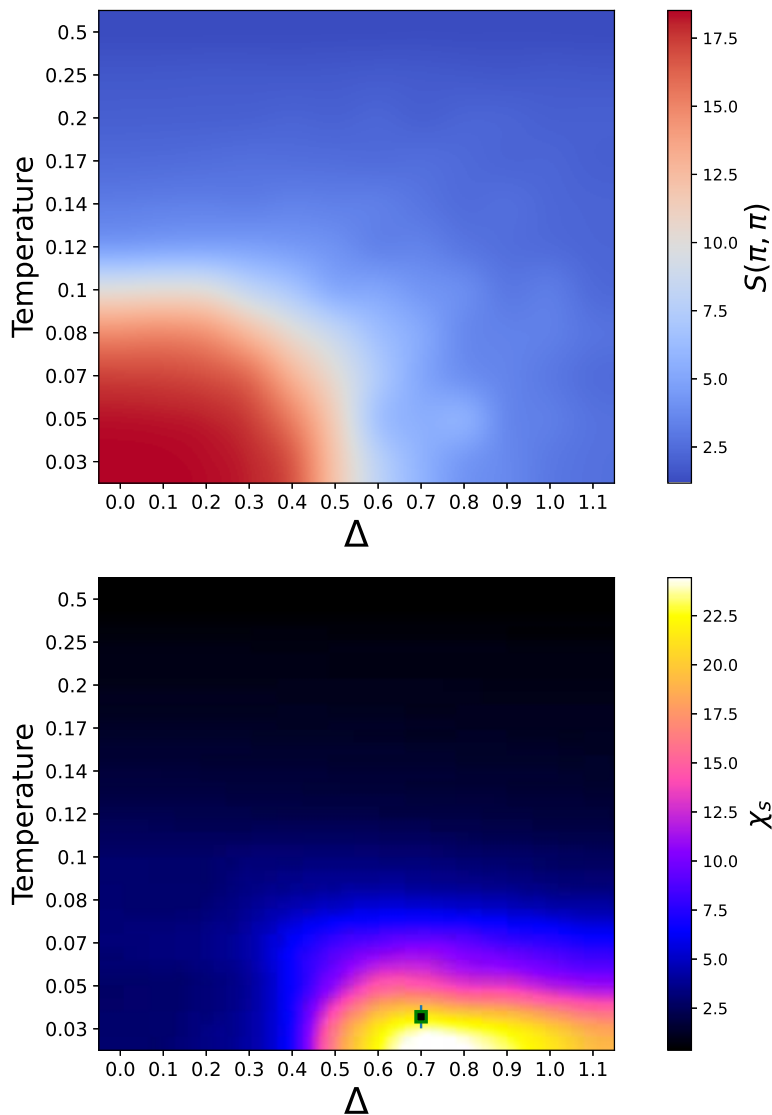
Figure S1. (a) Heat map of the charge structure factor at $\mathbf{q} = (\pi, \pi)$, and (b) the pairing susceptibility in the disorder strength-temperature space. Colors correspond to the magnitudes of $S(\pi, \pi)$ and χ_s after interpolation. Here $L = 10$, $\omega_0 = 4$ and $\lambda_D = 0.25$ ($g = 2$). To connect this raw heat map data to the onset of superconducting order, we show in the lower panel a symbol representing the transition temperature inferred from finite size scaling of χ_s for different L.

higher density. Indeed, this is one of the reasons the transition temperatures can be quite different in the Hubbard and Holstein cases (especially at smaller ω_0).

E: Specific Heat- The effect of disorder on the CDW phase can also be monitored using thermodynamic responses, most significantly, the specific heat $C(T)$. To this end, we fit the DQMC data for the energy per site to the following ansatz [59, 60]

$$E(T) = \omega_0 \left(\frac{1}{e^{\beta \omega_0} - 1} + \frac{1}{2} \right) + \sum_{n=1}^{M} c_n e^{-n\beta\delta} , \quad (6)$$

in which the parameters c_n and δ are adjusted to

minimize the deviation of the fitted curve to the data points. The first term is the bare energy of the quantum oscillators in the Holstein Hamiltonian, and the second term captures the electronic contributions. We then obtain $C(T)$ by differentiating the fitted expression, in which we typically set $M = 6$ to 8.

Results for the specific heat are shown in Fig. S3. In the clean limit, $\Delta = 0$, $C(T)$ has a broad peak at $T/t \sim 0.8$ corresponding to the temperature scale of pair formation [60], and a sharp peak at $T/t = 0.24 \pm 0.01$ which aligns well with the critical temperature for the CDW transition determined by the scaling of $S(\pi, \pi)$ (see Fig. S2 in the Appendix B). Similar two-peak structures
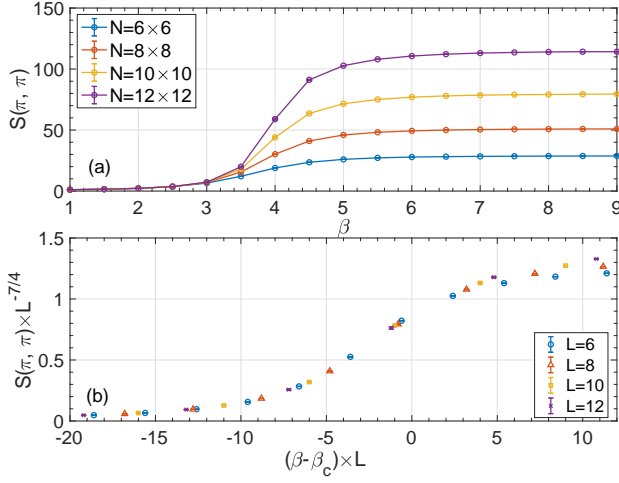
Figure S2. (a) The CDW structure factor as a function of inverse temperature β for four lattice sizes at $g = 1$ and $\omega_0 = 0.5$ (b) scaling collapse plot using 2D Ising critical exponents and $\beta_c = 4.1$.
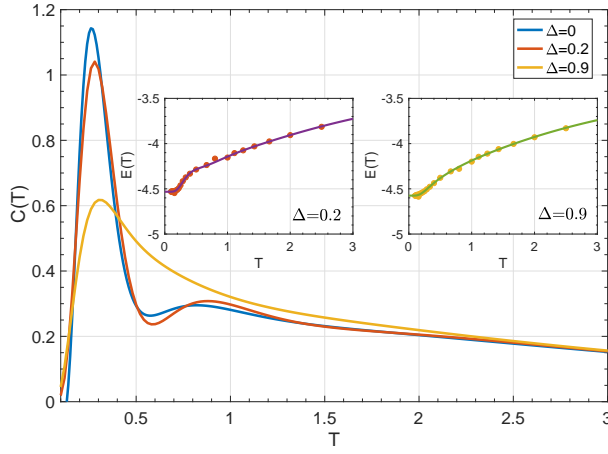

Figure S3. Specific heat $C(T)$ as a function of temperature for the clean system ($\Delta = 0$) and two values of disorder, fixing $L = 8$ and $\lambda_D = 0.5$ ($g = 1$). Inset: Raw data for the energy $E(T)$ and the fit given by Eq. 6 at $\Delta = 0.2$ and $\Delta = 0.9$.

are observed in the Hubbard model [60], and correspond in that case to the distinct energy scales of moment formation and antiferromagnetic ordering. At weak disorder, $\Delta/t = 0.2$, a sharp low temperature peak indicative of CDW formation persists. In fact, the peak is first shifted to slightly higher temperatures. Such an enhancement of T_c by disorder has been established in DQMC [61] and dynamical mean field theory [62] of the Anderson-Hubbard model. The effect arises from the initial growth of the exchange energy $J = 2t^2/(U + \Delta) + 2t^2/(U - \Delta) > 4t^2/U$ with random site energy. Precisely the same phenomenon might be expected here, since quantum fluctuations in the CDW phase have a similar form, with the pair binding energy $4g^2/\omega_0$ playing
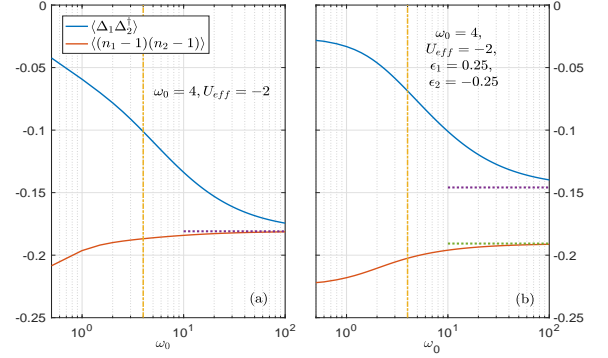

Figure S4. Nearest neighbor pairing and CDW correlations for the half-filled Holstein (solid curves) and attractive Hubbard (horizontal dashed lines at large ω_0) dimers. <u>Panel a:</u> Clean case where the two sites have identical site energies. Here the pairing and charge correlations are degenerate in the Hubbard limit. <u>Panel b:</u> 'Disordered' case with site energy difference $(\epsilon_1 - \epsilon_2)/t = 0.50$, of the same scale as the disorder studied in this paper. The effect of the site energy is to break the CDW-Pairing degeneracy (which is already broken in the clean Holstein model) also in the Hubbard limit. In both cases, the Hubbard limit is not reached until $\omega_0/t \gtrsim 10^2$.
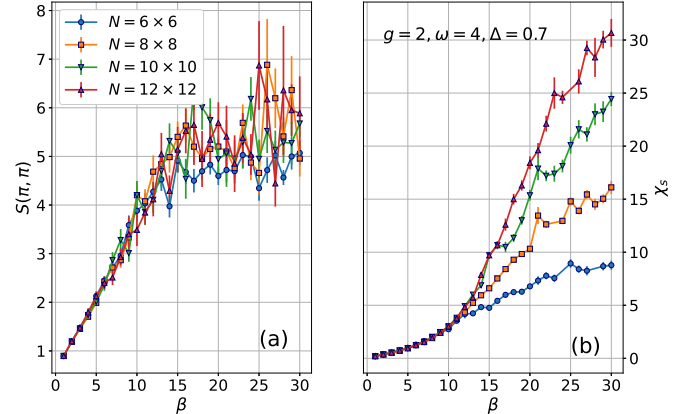

Figure S5. The (a) charge structure factor $S(\pi, \pi)$, and (b) s-wave pairing susceptibility χ_s as functions of the inverse temperature β, at fixed $\Delta = 0.7$. Here $\omega = 4$ and $\lambda_D = 0.25$ ($g = 2$).

the role of U. Further increase of Δ reduces the peak of the specific heat, in line with the suppression of the CDW order.

F: Temperature dependence in the anti-adiabatic regime- Fig. S5 shows results at $\Delta = 0.7$, near the optimal disorder, where the pairing susceptibility χ_s is largest in Fig. 3. Unlike Fig. S2, $S(\pi, \pi)$ no longer grows with N at low temperature, as seen in Fig. S5(a).

However, as shown in Fig. S5(b), χ_s grows with lattice size, indicating the presence of robust superconducting correlations in an intermediate disorder window. The result of the scaling analysis of these data is presented in the inset of Fig. 3.

The combination of the destruction of CDW order and the rise in SC order illustrated in the temperature evolution of Fig. S5, together with the suppression of $S(\pi, \pi)$ and the onset of χ_s of Fig. 3 indicates a competition between the two types of order [29]. The possibility of a cooperation, in which CDW fluctuations mediate pairing, has been discussed in [63].

G: Disorder dependence in the adiabatic regime- In Fig. S6 we re-plot the data in the adiabatic regime from Fig. 1 emphasizing the evolution with disorder. The sharp drop in $S(\pi, \pi)$ at $\Delta \sim 0.5$ corresponds to the destruction of CDW order, with no SC phase. A further signal of the transition is seen in the kinetic energy, which becomes smaller in magnitude upon exiting the CDW phase since virtual hopping is reduced when sites with electron pairs are no longer surrounded exclusively by empty sites.

H: Analytic Continuation Method- We perform the calculation of $A(\omega)$ using the maximum entropy approach [64–66]. This method determines the spectral function by a weighting which combines a Gaussian piece measuring

the deviation of a computed $G(\tau)$ from the QMC values for a given $A(\omega)$, and an entropic piece, with a relative coefficient determined by Bayesian logic. We use the most straightforward implementation with a flat default model (the $A(\omega)$ which would result in the absence of data), and only the diagonal elements of the covariance matrix associated with measuring G at two different imaginary time values.

I: Susceptibility Histograms- More detail concerning the enhancement of pairing by disorder is given by the histograms of the susceptibility of Fig. S7. The figure also gives a sense for the realization-to-realization fluctuations in χ_s.
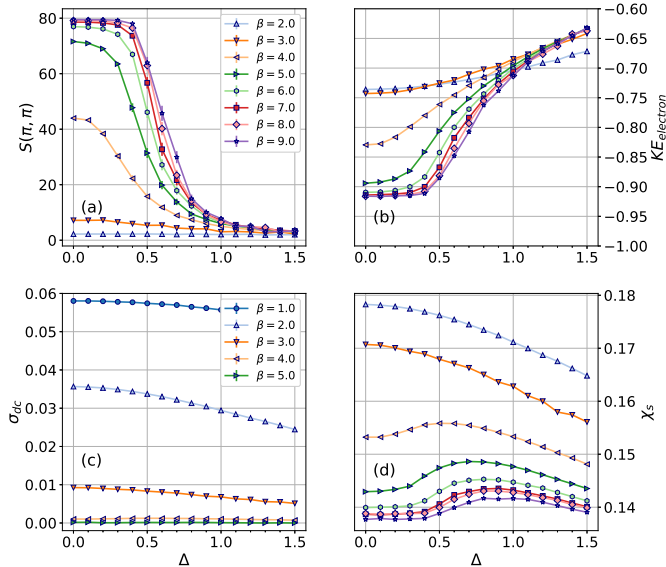

Figure S6. Disorder dependence of charge structure factor $S(\pi, \pi)$, the electron kinetic energy $KE_{electron}$, dc conductivity σ_{dc} and s-wave pairing susceptibility, panels a-d, respectively at fixed $L = 10$. Here $\omega_0 = 0.5$ and $\lambda_D = 0.5$ ($g = 1$).
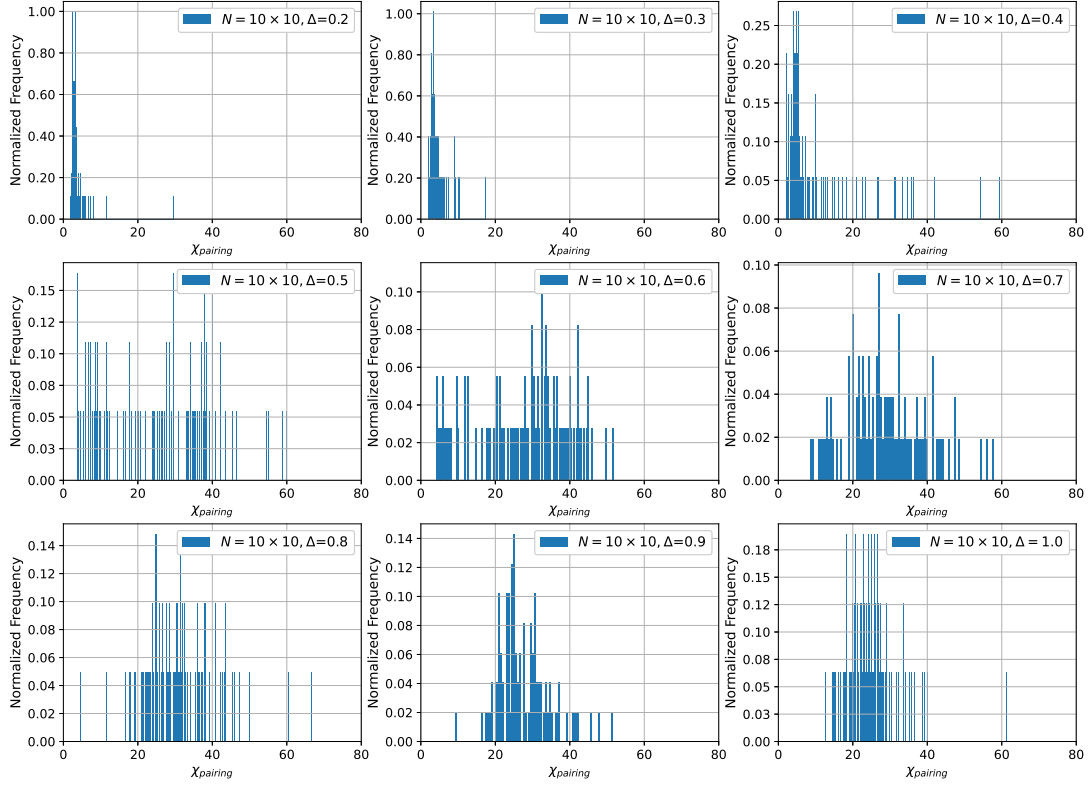
Figure S7. Histograms of distinct realizations of the pairing susceptibility for different disorder strengths Δ. For small Δ, a single narrow peak occurs at small χ_s. As Δ increases, the distribution broadens and shifts to large values. This is the intermediate superconducting phase. At the largest Δ, the distribution begins returning to smaller values of pairing; superconductivity is suppressed.